OPTIMIZATION OF AKM FIRING ATTITUDE

M. Hirota A. Tanaka

Tsukuba Space Center
National Space Development Agency
Ibaraki, Japan

C. Abe T. Shimizu

Fujitsu Limited
Tokyo, Japan

ABSTRACT

The drift orbit realized by AKM ignition is usually deviated from the planned one due to the small residuals of the AMF parameters. For the solid AKM, the controllable parameters at AMF are the firing time and the attitude of the spin axis. The firing time is so determined as to obtain the desired drift orbital plane, and AMF time error is negligible in the usual cases. Therefore the residuals of the AKM velocity increment and the AMF attitude must be taken into consideration in order to optimize the AMF attitude. The optimum AMF attitude is defined as the minimax one which minimizes the maximum stationing fuel on the surface of the ellipsoid defined by the AMF velocity increment vector error. For the purpose of saving the stationing fuel, two techniques are taken into consideration; one is utilization of the velocity increment caused by the reorientation maneuver, and the other is adoption of post-burn maneuver by the axial thruster.

Keywords: AKM Firing Attitude, Velocity Increment by AKM, Geostationary Radius, Drift-Rate, Eccentricity Vector, Inclination Vector, Post-Burn, Apsis Bias

1. INTRODUCTION

Because Apogee Kick Motor (AKM) firing is the most important maneuver which injects the satellite from the transfer orbit into the drift orbit, AKM firing (AMF) attitude must be carefully selected in order to minimize the fuel necessary for stationing maneuvers. Optimum AKM firing attitude is defined as the minimax one which minimizes the maximum fuel on the error ellipsoid of the controllable parameters. In this paper, the following conditions are supposed:

- . orbit determination error is negligible, and
- . velocity increment of AKM is fixed (i.e. solid AKM).

This paper presents the following:

- . error propagation from the AMF parameters to the drift orbital elements,
- . some geometrical solutions of the AMF attitude which give the typical drift orbits, and
- . some techniques to optimize the AMF attitude.

2. PRELIMINARY AMF PLANNING

Supposing that the drift-rate control and the inclination control are carried out in the independent maneuvers and any errors at AKM ignition are not taken into consideration, the optimum AMF plan is such one to attain the desired orbital plane. That is, AKM must be ignited on the crossing line determined by the transfer orbital plane and the desired drift orbital plane. The general view of the preliminary AMF planning is shown in Fig. 1. P is AMF point and AKM velocity traces the circle C on the drift orbital plane. In this paper, we introduce the rectangular coordinate system on the drift orbital plane as described in Fig. 1, where E gives the drift orbit of zero eccentricity, and y-axis is orthogonal to $\vec{r}$.

The preliminary AMF planning is equivalent to obtain the optimum point on the circle C such as the fuel minimum, the eccentricity minimum, and so on.

However some residuals of AMF parameters and some restrictions in the actual operation must be taken into consideration.

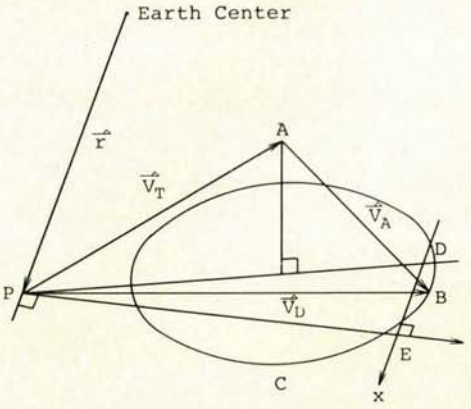

$\vec{r}$: Satellite Position Vector
$\vec{V}_T$: Velocity Vector of Transfer Orbit
$\vec{V}_A$: Increment Velocity Vector by AKM
$\vec{V}_D$: Velocity Vector of Drift Orbit

Figure 1. Preliminary AKM Firing Planning

Proc. Int. Symp. Spacecraft Flight Dynamics, Darmstadt, FRG, 18-22 May 1981 (ESA SP-160, Aug. 1981)

3. EFFECT OF AMF PARAMETER ERRORS

The AMF parameters are as follows:

- . AMF time,
- . AKM size (i.e. velocity increment), and
- . AMF attitude.

3.1 Description of the drift orbital elements

Because the eccentricity and the inclination are nearly equal to zero, the drift orbit is completely represented by the mean longitude of the subsatellite point, the drift-rate, the eccentricity vector, and the inclination vector. They are defined as follows, where the dot means the time differentiation:

$$\lambda = \Omega + \omega + M - \theta_g, \tag{1}$$

$$\dot{\lambda} = \dot{\Omega} + \dot{\omega} + \dot{M} - \dot{\theta}_g, \tag{2}$$

$$\vec{e} = \begin{pmatrix} \xi \\ \eta \end{pmatrix} = e \begin{pmatrix} \cos(\Omega+\omega) \\ \sin(\Omega+\omega) \end{pmatrix}, \tag{3}$$

$$\vec{i} = \begin{pmatrix} p \\ q \end{pmatrix} = \sin i \begin{pmatrix} \cos\Omega \\ \sin\Omega \end{pmatrix}, \tag{4}$$

λ : mean longitude of the subsatellite point,
$\dot{\lambda}$: drift-rate,
$\vec{e}$: eccentricity vector, e: eccentricity,
$\vec{i}$: inclination vector, i: inclination,
Ω : right ascension of ascending node,
ω : argument of perigee, and
θ_g: Greenwich sidereal time.

3.2 Jacobian matrix

In the equatorial coordinate system, the position vector $\vec{r}$ and the velocity vector $\vec{V}$ are expressed in terms of the Keplerian elements as follows:

$$\vec{r} = a \begin{pmatrix} \cos\Omega & -\sin\Omega & 0 \\ \sin\Omega & \cos\Omega & 0 \\ 0 & 0 & 1 \end{pmatrix} \begin{pmatrix} 1 & 0 & 0 \\ 0 & \cos i & -\sin i \\ 0 & \sin i & \cos i \end{pmatrix} \times \begin{pmatrix} \cos\omega & -\sin\omega & 0 \\ \sin\omega & \cos\omega & 0 \\ 0 & 0 & 1 \end{pmatrix} \begin{pmatrix} \cos E - e \\ \sqrt{1-e^2}\sin E \\ 0 \end{pmatrix}, \tag{5}$$

$$\vec{V} = \sqrt{\frac{\mu a}{r}} \begin{pmatrix} \cos\Omega & -\sin\Omega & 0 \\ \sin\Omega & \cos\Omega & 0 \\ 0 & 0 & 1 \end{pmatrix} \begin{pmatrix} 1 & 0 & 0 \\ 0 & \cos i & -\sin i \\ 0 & \sin i & \cos i \end{pmatrix} \times \begin{pmatrix} \cos\omega & -\sin\omega & 0 \\ \sin\omega & \cos\omega & 0 \\ 0 & 0 & 1 \end{pmatrix} \begin{pmatrix} -\sin E \\ \sqrt{1-e^2}\cos E \\ 0 \end{pmatrix}, \tag{6}$$

where μ is geogravitational constant, and $r=|\vec{r}|$. Noticing that the inclination and the eccentricity are nearly equal to zero, the Jacobian matrix from the $(\vec{r}, \vec{V})$ coordinate system to the $(a,\lambda,\vec{e},\vec{i})$ coordinate system is obtained as follows:

$$\frac{\partial \begin{pmatrix} a \\ \lambda \\ \xi \\ \eta \\ p \\ q \end{pmatrix}_{\theta_g=0}}{\partial \begin{pmatrix} \vec{r} \\ \vec{V} \end{pmatrix}} \fallingdotseq \begin{pmatrix} 2\cos\lambda & 2\sin\lambda & 0 \\ \frac{1}{a}\sin\lambda & -\frac{1}{a}\cos\lambda & 0 \\ \frac{1}{a}\cos 2\lambda & \frac{1}{a}\sin 2\lambda & 0 \\ \frac{1}{a}\sin 2\lambda & -\frac{1}{a}\cos 2\lambda & 0 \\ 0 & 0 & \frac{1}{a}\sin\lambda \\ 0 & 0 & -\frac{1}{a}\cos\lambda \\ -\frac{2}{n}\sin\lambda & \frac{2}{n}\cos\lambda & 0 \\ -\frac{2}{n}\cos\lambda & -\frac{2}{na}\sin\lambda & 0 \\ -\frac{1}{2na}\sin 2\lambda & \frac{1}{2na}(\cos 2\lambda+3) & 0 \\ \frac{1}{2na}(\cos 2\lambda-3) & \frac{1}{2na}\sin 2\lambda & 0 \\ 0 & 0 & \frac{1}{na}\cos\lambda \\ 0 & 0 & \frac{1}{na}\sin\lambda \end{pmatrix} \tag{7}$$

3.3 Error propagation to the drift orbit

In this section, the subscript T presents the element of the transfer orbit and the prime sign means the rotation of $(\vec{r},\vec{V})$ coordinate by $\Omega_T+\omega_T$ or Ω_T. Because the AKM is ignited near the apogee, the deviation of the eccentric anomaly E by the AMF time t is approximated by

$$\frac{dE}{dt} \fallingdotseq \frac{n_T}{1+e_T}, \tag{8}$$

where n is the mean motion. Therefore the deviation of the AMF points by the AMF timing error is presented by

$$\Delta\vec{r}' \fallingdotseq a_T\sqrt{\frac{1-e_T}{1+e_T}}\, n_T\Delta t \begin{pmatrix} 0 \\ \cos i_T \\ \sin i_T \end{pmatrix}. \tag{9}$$

The deviation of the velocity vector is given by

$$\Delta\vec{V}' \fallingdotseq \sqrt{\frac{\mu}{a_T}}\frac{n_T\Delta t}{(1+e)^2}\begin{pmatrix} -1 \\ 0 \\ 0 \end{pmatrix} + V_A \begin{pmatrix} -\cos\delta\cdot\Delta\alpha \\ -\sin\delta\cdot\Delta\delta \\ \cos\delta\cdot\Delta\delta \end{pmatrix} + \Delta V_A \begin{pmatrix} 0 \\ \cos\delta \\ \sin\delta \end{pmatrix}, \tag{10}$$

where α, δ, and V_A present right ascension and declination of the AMF attitude and velocity increment of AKM respectively.
The deviations of the drift orbital elements are obtained as follows:

$$\Delta\begin{pmatrix} a \\ \lambda \\ \xi' \\ \eta' \\ p' \\ q' \end{pmatrix} \fallingdotseq \frac{\partial \begin{pmatrix} a \\ \lambda \\ \xi' \\ \eta' \\ p' \\ q' \end{pmatrix}_{\lambda=0}}{\partial \begin{pmatrix} \vec{r}' \\ \vec{V}' \end{pmatrix}} \cdot \Delta\begin{pmatrix} \vec{r}' \\ \vec{V}' \end{pmatrix}. \tag{11}$$

The detailed description of each deviation appears in the corresponding subsection.

3.3.1 Semi-major axis and mean longitude. The deviations of the semi-major axis a and the mean longitude λ are approximated by

$$\Delta\begin{pmatrix} a \\ \lambda \end{pmatrix} \fallingdotseq \begin{pmatrix} \frac{2a_D}{V_D}(-V_A\sin\delta\cdot\Delta\delta + \Delta V_A\cos\delta) \\ \frac{n_T\cdot\Delta t}{\sqrt{(1+e_T)^3}}(2-\sqrt{1-e_T}\cos i_T) + \frac{2V_A}{V_D}\cos\delta\cdot\Delta\alpha \end{pmatrix}, \tag{12}$$

where subscript D presents the element of the drift orbit and V_D is mean velocity defined by

$$V_D = \sqrt{n_D a_D} = \sqrt{\frac{\mu}{a_D}} \quad . \tag{13}$$

3.3.2 Eccentricity vector. The deviation of $\vec{e}$ is given by

$$\Delta\begin{pmatrix}\xi'\\ \eta'\end{pmatrix} = \begin{pmatrix} \frac{2}{V_D}(-V_A \sin\delta\cdot\Delta\delta + \Delta V_A \cos\delta) \\ \frac{n_T\cdot\Delta t}{\sqrt{(1+e_T)^3}}(1-\sqrt{1-e_T}\cos i_T) + \frac{V_A}{V_D}\cos\delta\cdot\Delta\alpha \end{pmatrix}, \tag{14}$$

where the prime sign means the rotation by $\Omega_T+\omega_T$. The feature of the deviation of $\vec{e}$ is shown in Fig. 2.

3.3.3 Inclination vector. The deviation of $\vec{i}$ is presented by

$$\Delta\begin{pmatrix}p'\\ q'\end{pmatrix} = \begin{pmatrix} \frac{1}{V_D}(V_A \cos\delta\cdot\Delta\delta + \Delta V_A \sin\delta) \\ -\sqrt{\frac{1-e_T}{1+e_T}}\; n_T\Delta t\cdot\sin i_T \end{pmatrix},$$

where the prime sign means the rotation by ΩT. The feature of the deviation of $\vec{i}$ is shown in Fig. 3.

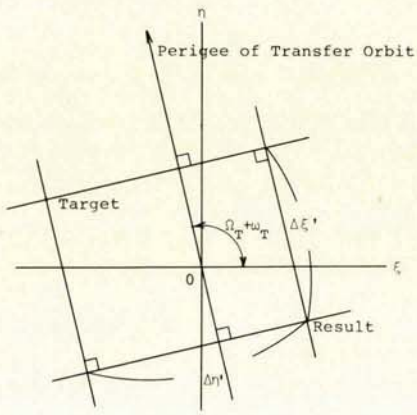

Figure 2. Deviation of Eccentricity Vector

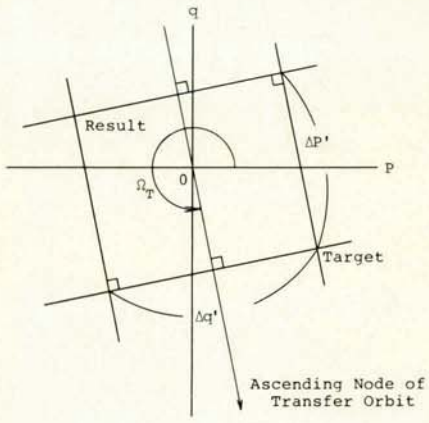

Figure 3. Deviation of Inclination Vector

4. TYPICAL DRIFT ORBITS

There are some characteristic points on the circle C in Fig. 1 which correspond to some typical drift orbits. They are as follows:

i) maximum semi-major axis,
ii) minimum eccentricity, and
iii) zero apsis bias.

Apsis bias is defined as the difference between the apsis radius and the geostationary radius. Geometrical descriptions of these characteristic points appear below.

4.1 Maximum semi-major axis

The point, which gives the maximum semi-major axis of the drift orbit, corresponds to the maximum velocity vector on the circle C in Fig. 1. This point is presented as D in Fig. 1.

4.2 Maximum eccentricity

The deviation of $\vec{e}$ by $\Delta\vec{V}$ is given by

$$\Delta\begin{pmatrix}\xi'\\ \eta'\end{pmatrix} = \frac{\partial\begin{pmatrix}\xi\\ \eta\end{pmatrix}_{\lambda=0}}{\partial(\vec{V})}\cdot\Delta\vec{V}' \quad . \tag{16}$$

In the x-y coordinate system in Fig. 1, the equi-eccentricity curve is presented by

$$e_D = \sqrt{(\Delta\xi')^2+(\Delta\eta')^2} = \frac{1}{V_D}\sqrt{x^2+(2y)^2} \quad . \tag{17}$$

As shown in Fig. 4, minimum eccentricity of the drift orbit is realized by the contact point F of the circle C and the ellipse described by Eq.(17). In Fig. 4, point G gives the zero flight path angle of the drift orbit at the AMF point. Notice that G is very close to F because the center of the circle C lies almost on the y-axis (cf. Fig. 1).

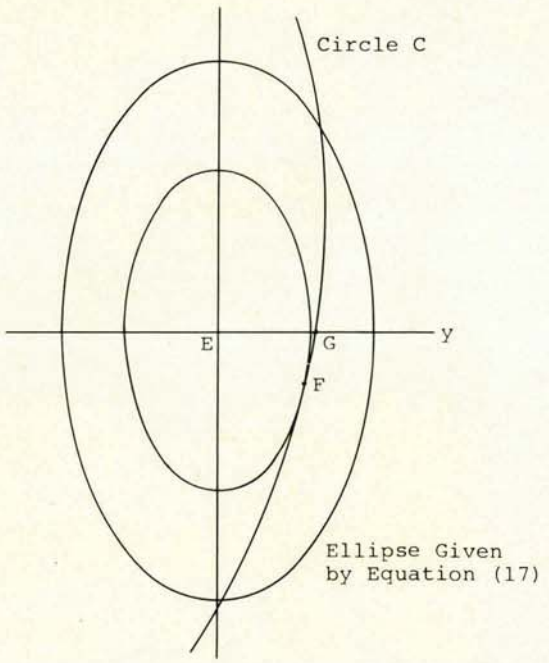

Figure 4. Minimum Eccentricity

4.3 Zero apsis bias

Zero apsis bias is described as

$$a_D \cdot (1 \pm e_D) = r_S \ , \tag{18}$$

where subscript S presents the element of the geostationary orbit. a_D is described as

$$V_D = \sqrt{x^2 + (V_E + y)^2} = \sqrt{\mu\left(\frac{2}{r} - \frac{1}{a_D}\right)}, \text{ with} \tag{19}$$

$$V_E = \sqrt{\frac{\mu}{r}} \ , \tag{20}$$

and approximately as

$$a_D \fallingdotseq r\left[1 + \frac{1}{V_E^2}(x^2 + 2V_E y + 5y^2)\right] \tag{21}$$

e_D is obtained as

$$e_D = \sqrt{\left(\frac{rV_D^2}{\mu} - 1\right)^2 \cos^2\beta + \sin^2\beta}$$
$$\fallingdotseq \sqrt{\frac{x^2+4y^2}{V_E^2} + \frac{2x^2y+4y^3}{V_E^3} + \frac{x^2y^2+y^4}{V_E^4}} \ , \tag{22}$$

where β is flight path angle. From Eq.(18),(21), and (22) the following equation is reduced:

$$y \fallingdotseq \frac{2\frac{r_S}{r} - 1}{4V_E\left(1 - \frac{r_S}{r}\right)} x^2 - \frac{V_E\left(1 - \frac{r_S}{r}\right)}{4} \tag{23}$$

and this parabolla is depicted in Fig. 5, where H and I present the points which realize the drift orbit with zero apsis bias. In case of no crossing point, apsis bias zero is not realized. The semi-major axis becomes larger as nearer as the point approaches to the point D.

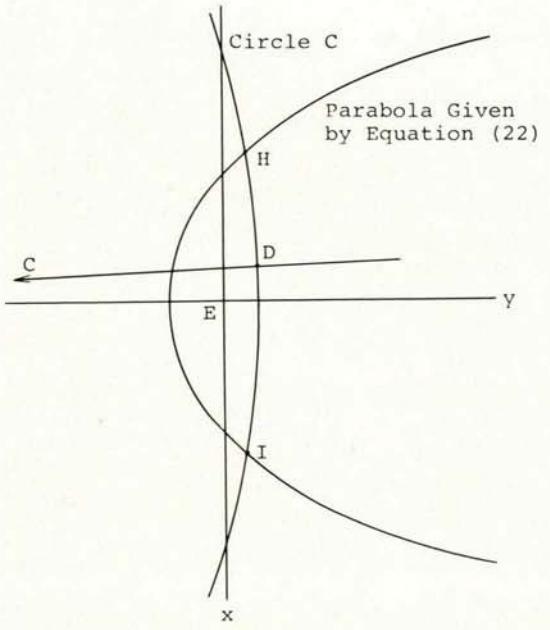

Figure 5. Zero Apsis Bias

5. ESTIMATION OF STATIONING FUEL

The stationing maneuver operations are restricted by the constraints such as:

i) visibility zone of the tracking and control stations in Japan,
ii) maximum magnitude of each orbital maneuver, and
iii) available time for stationing.

The first restriction is characteristic to the tracking and control network in Japan (see Ref. 1). For the purpose of obtaining the operationable station acquisition sequence, the special type of the station acquisition planning chart has been developed.

5.1 Station acquisition planning chart

The station acquisition planning chart is the conjunction of two charts as shown in Fig. 6 or 7, where one chart describes $(\lambda, \dot{\lambda})$ and the other presents two apsis biases, namely, Bx and By. Notice that (Bx,By) coordinate is rotated by 135° in order to conjunct two chart by the drift-rate scale.

5.2 Station Acquisition sequence

Two different types of the station acquisition sequences are constructed corresponding to the signs of Bx·By.

5.2.1 Bx·By>0 case. Fig. 6 depicts the feature of Bx·By>0 case, where λ_1 and λ_2 present the most west and most east station longitudes respectively. The former attains the fastest sequence although the latter corresponds to the slowest one. Notice that the stationing fuel is minimized for both cases. If the station longitude lies between λ_1 and λ_2, the station acquisition sequence minimizes the stationing fuel. We call this sequence "Normal Sequence". If the station longitude exsists westward of λ_1 or eastward of λ_2, some additional fuel is necessary for stationing. We call this case "Drift-back Sequence" or "Drift-up Sequence" respectively. The additional fuel is obtained by considering the drift of the satellite from λ_1 or λ_2 to the station during the available time restricted by iii). Thus the actual maneuver sequence can be simulated taking all constraints as described above into consideration.

5.2.2 Bx·By<0 case. Fig. 7 shows the feature of the Bx·By<0 case, where λ_1 and λ_2 have the same meaning as described in 5.2.1. But notice that these two sequences correspond to the slowest ones.

6. POST-BURN

For the purpose of saving the stationing fuel, the post-burn maneuver can be taken into consideration. In this paper we suppose that the post-burn maneuver is carried out at the AMF attitude by the axial thruster. This technique is useful not only for the recovery of the off-nominal transfer orbit but also for the correction of the drift orbit errors caused by the AMF parameter errors.

6.1 Classification of post-burn maneuvers

For the classification of the post-burn maneuvers, the following features of the drift orbit must be taken into consideration, namely, signs of the apsis biases, inclination vector, and mounting

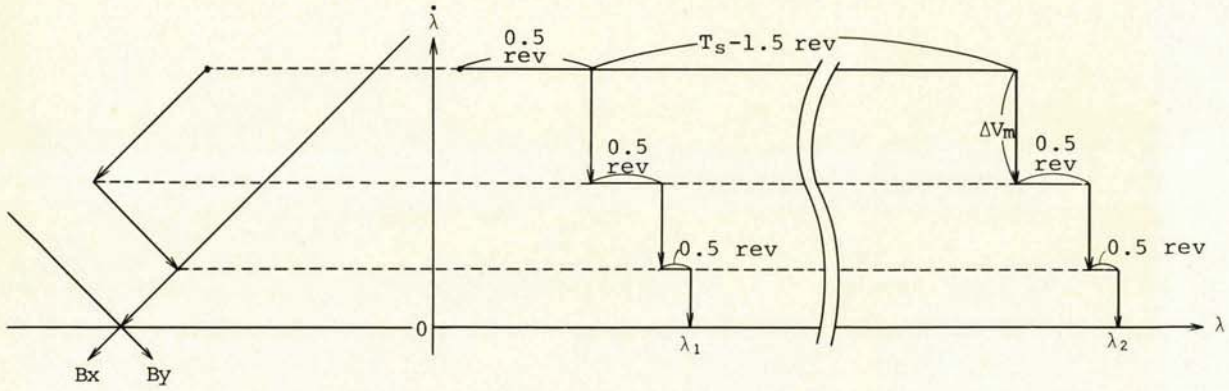

ΔV_m: Maximum Magnitude of One Maneuver
T_s: Available Period for Stationing

Figure 6. Example of Reference Acquisition Sequences (Bx·By>0)

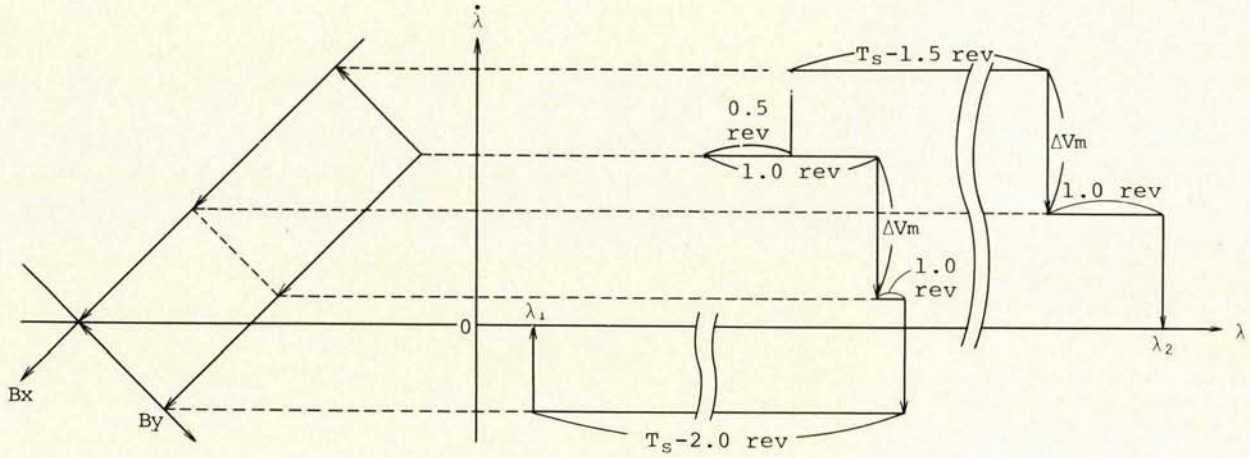

ΔV_m: Maximum Magnitude of One Maneuver
T_s: Available Period for Stationing

Figure 7. Example of Reference Acquisition Sequences (Bx·By<0)

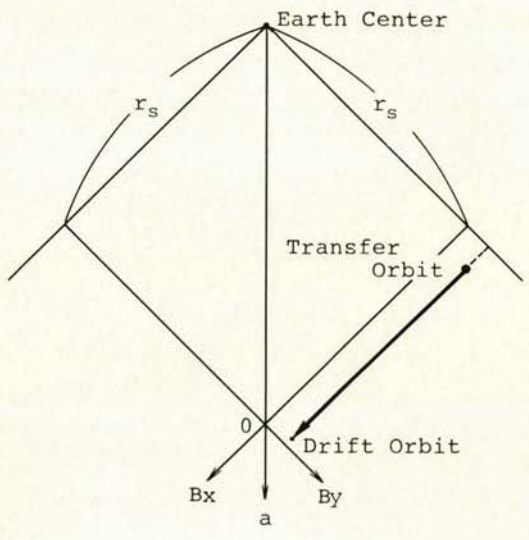

Figure 8. Illustration of AKM Firing in Apsis Biases Chart

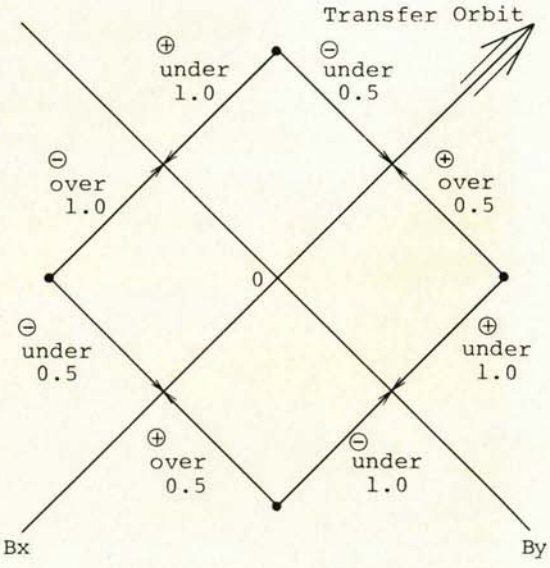

Figure 9. Several Types of Post-Burn

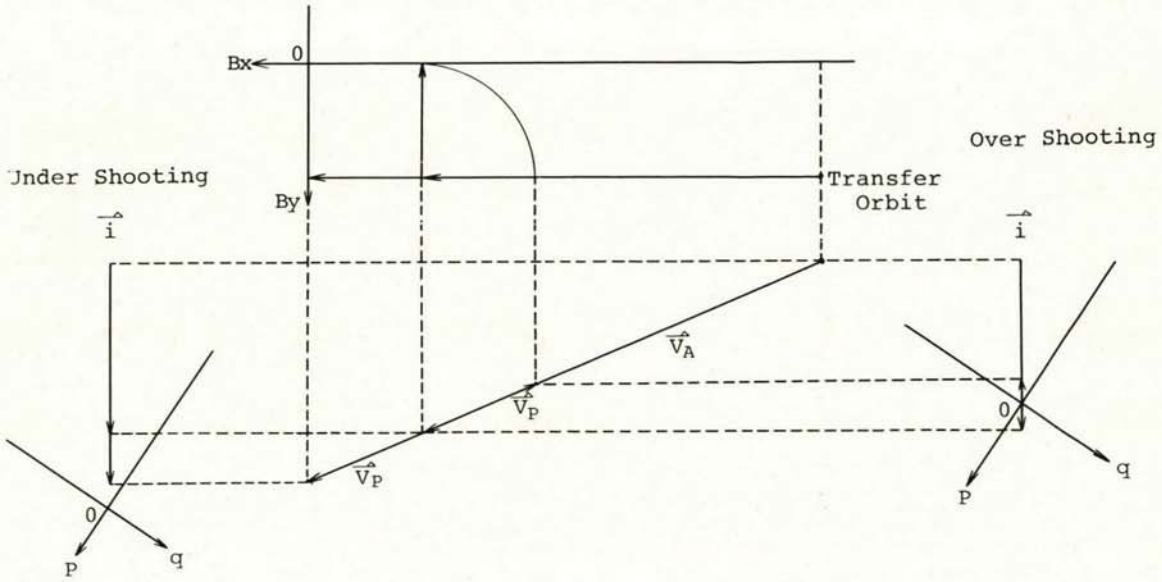

Figure 10. Example of Post-Burn Planning

angle of the axial thruster. Fig. 8 shows the AMF event represented in the Bx-By chart, where the bold arrow presents the velocity increment vector on the Bx-By plane. The detailed feature of Fig. 8 is shown in Fig. 9, where the several types of the post-burn maneuvers are depicted. The post-burn velocity vector must be parallel or anti-parallel corresponding to the ⊕ or ⊖ sign respectively. 'over' and 'under' present the 'over-shooting' and 'under-shooting' of the AMF velocity vector when depicted in (p,q) plane respectively. '0.5' and '1.0' present the post-burn time in revolution of the drift orbit after the AKM ignition.

6.2 Post-burn planning

Two illustrative examples of the post-burn planning are shown in Fig. 10, where $\hat{V}_P$ represent the post-burn velocity vector. The left example is classified in (under,⊕,1.0), although the right one belongs to the (over,⊖,0.5) class.

7. OPTIMUM AMF ATTITUDE

For the optimization of the AMF attitude, the following items must be taken into consideration:

i) residuals of the AMF parameters,
ii) operational constraints for the stationing maneuvers,
iii) effect of the attitude reorientation maneuver, and
iv) post-burn.

Among the AMF parameters, only the residual of the AMF velocity increment vector is taken into consideration because the AMF timing error is negligible.

7.1 Restriction-free case

The optimization technique results in the selection of the characteristic points as described in the section 4 if no restriction is taken into consideration. All optimum points are classified in Table 1 corresponding to the given transfer orbits. Those features are depicted in Fig. 11.

Table 1. Optimum Point

Case	r	Circle & Parabola	a maximum	Optimum Point
1	$\geq r_s$	crossing		bias zero (a minor)
2		not crossing		e minimum
3			Outside of parabola	
4	$< r_s$		inside of parabola	a maximum
5		crossing		
6			Outside of parabola	bias zero (a major)

7.2 Restriction by velocity vector error

The stationing fuel is mainly affected by V_A and δ. Supposing that the inclination correction and in-plane maneuvers are performed separately, the optimum point T is obtained as shown in Fig. 12. T is presented as the center of the error ellipse determined by ΔV_A and $V_A \Delta\delta$. For the reference, point J corresponds to the optimum attitude for the restriction-free case.

7.3 Reorientation and post-burn

Because the time of the reorientation is arbitrary, it should be so selected as to minimize the stationing fuel. Supposing that the attitude vector moves on the great circle and the axial thruster is mounted anti-parallel to the spin axis, the velocity increment V_R is given by

$$V_R = \frac{2I_S\omega_S}{M_S h} \sin\frac{\theta}{2} , \qquad (24)$$

where I_S is moment of inertia, ω_S is spin-rate, M_S is mass of the satellite, h is moment arm, and θ is the precession angle. The direction of V_R is determined by the vector sum of the initial and final

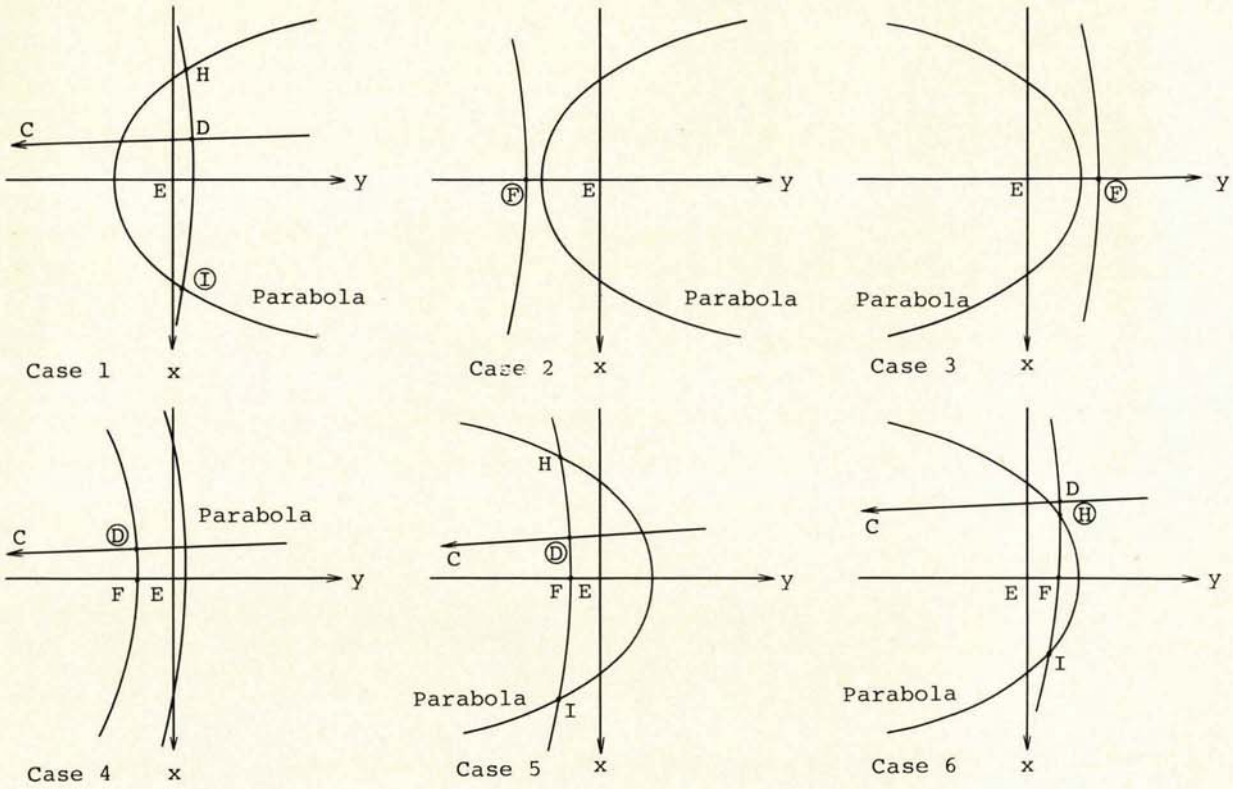

Figure 11. Optimum Points for Stationing (Restriction Free Case)

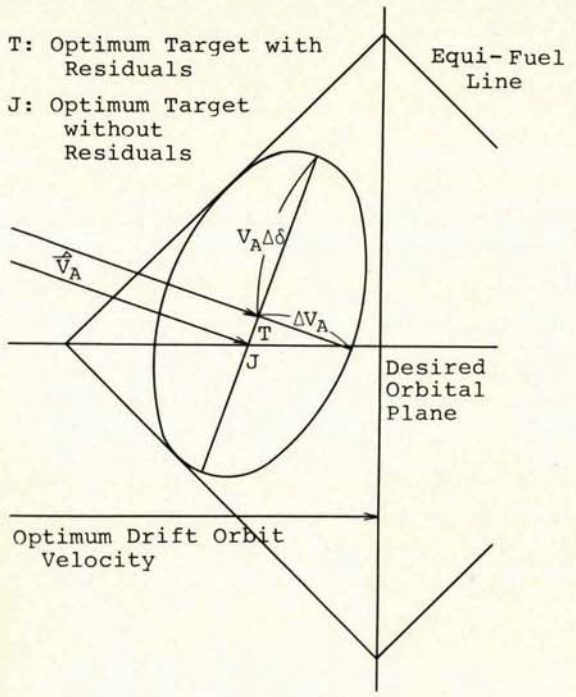

Figure 12. Optimum Target Considering Residuals in AKM Firing Parameters

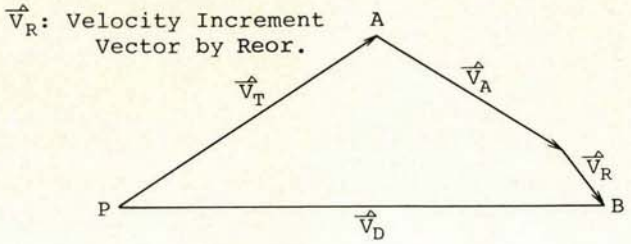

Figure 13. Example of Effect of Attitude Reorientation

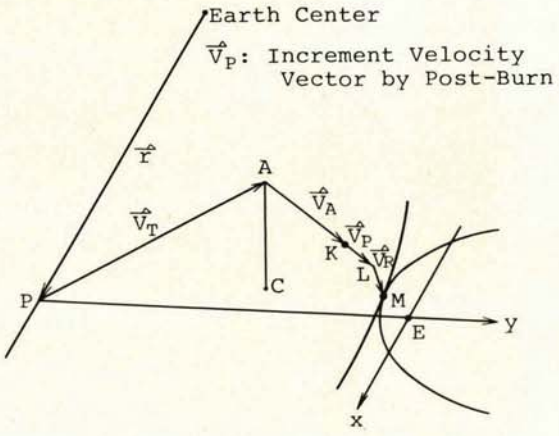

Figure 14. Initial Value of Calculation

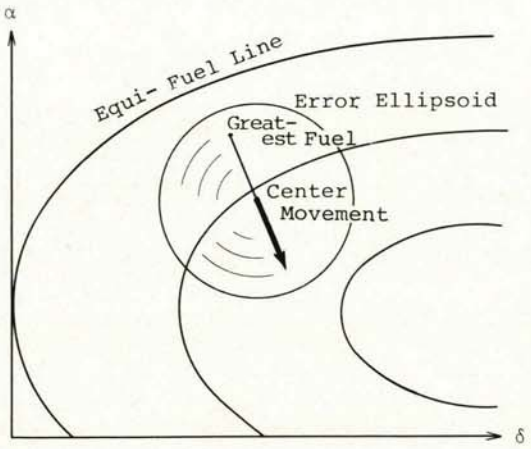

Figure 15. Optimization

spin vectors. An illustrative example is shown in Fig.13 as the 'under shooting' case. The reorientation must be executed at the AMF point for this case. The effect of the post-burn maneuver is similar to that of the reorientation maneuver.

7.4 Optimization procedure

All items mentioned above should be taken into consideration to obtain the optimum AMF attitude. For this purpose, an iterative method is adopted as described below.

7.4.1 Initial value. As the initial value of the AMF attitude, we select the contact point of the modified circle C and the parabolla defined by the Eq. (23). The feature of the initial point is depicted in Fig. 14. Notice that the effect of the reorientation and post-burn maneuvers are taken into consideration.

7.4.2 Stationing fuel calculation. The stationing fuel is obtained by the following procedure;
1) obtain the reorientation time,
2) obtain the post-burn time,
3) simulate the AMF including the reorientation and post-burn maneuvers,
4) calculate the fuel for the in-plane stationing maneuvers taking the operational constraints into consideration,
5) calculate the fuel for the inclination correction maneuver, and
6) obtain the total stationing fuel taking all maneuvers described above into consideration.

7.4.3 Iterative procedure. Because the AMF time is uniquely determined to attain the desired drift orbital plane, the controllable parameters are only the AMF attitude elements. Taking the residuals of AMF velocity vector into consideration, the optimum AMF attitude is obtained by the procedure as follows;
1) calculate the stationing fuel corresponding to the point on the surface of the error ellipsoid,
2) obtain some characteristic points which give the maximum stationing fuels,
3) compare the maximum values obtained by the step 2,
4) if the difference among the values described above is less than the tolerance, then the optimum point is obtained, and
5) else, move the center to the opposit point (see Fig. 15) and go to the step 1.

8. CONCLUSION

The optimum AMF attitude is obtained taking the residuals of the AMF parameters, the operational constraints for stationing, and the effects of the reorientation and post-burn maneuvers into consideration. This method has been reduced for the tracking and control software, which is ready for the future geostationary satellite missions of Japan.

9. ACKNOWLEDGEMENTS

The authors would like to thank Dr.T.Takenouchi, Mr.M. Utashima, and Mr. T. Babauchi for their helpfull discussions and Mr.K.Yoneyama and Mr. T. Ogino for their reviews on this paper.

10. REFERENCES

1. Suzuki M et al 1981, NASDA tracking and control system, Proc. of International Symposium on Spacecraft Flight Dynamics, Darmstadt 18-22 May 1981.

2. Tanaka A et al 1981, Mission analysis for maneuver, Proc. of International Symposium on Spacecraft Flight Dynamics, Darmstadt 18-22 May 1981.

3. Hirota M et al 1978, Mathematical model description for maneuver programs (in Japanese), NASDA.